

A distributed optical fiber sensor for temperature detection in power cables

Gunes Yilmaz*, Sait Eser Karlik

Department of Electronics Engineering, Faculty of Engineering and Architecture, Uludag University, 16059 Gorukle, Bursa, Turkey

Received 29 November 2004; received in revised form 3 June 2005; accepted 20 June 2005

Available online 18 August 2005

Abstract

The power transfer capacity of an underground power cable is limited by high-temperature regions that occur along the cable. It is very difficult to determine and control these ‘hot spots’. Optimum use and temperature profile control of power cables before and during load transmission can be achieved with real-time processing of temperature data. There are various methods developed for this purpose such as conventional point temperature measurement method, where a large number of sensors and connectors are required, and methods based on mathematical models which can only approach real values by approximation.

In this study, temperature detection in an XLPE insulated 154 kV power cable is performed using a distributed sensing method where the optical fiber itself behaves as a sensor. Therefore, there is no need for the devices of conventional method. Moreover, contrary to methods based on mathematical models, where it is difficult to predict environmental variations, this method considers the variations with a temperature resolution of ± 1 °C. Distributed temperature sensing (DTS) method, detection system configuration and required system parameters are explained in the paper. Experimental results obtained for 126 and 412 m cables show a temperature resolution of ± 1 °C and a spatial resolution of 1.22 m. Simulations for a 10 km cable are also given. Results show that DTS is a reliable method for both short and long range cable systems.

© 2005 Elsevier B.V. All rights reserved.

Keywords: Raman sensor; Power cable; Distributed temperature sensing; OTDR; Fiber

1. Introduction

Power cable systems must be reliable and economical for a minimum period of 25 or 30 years since high voltage transmission and distribution systems require expensive investments. However, an underground power cable is exposed to electrical, thermal and mechanical effects during its operating time. These effects can damage the cable insulation. Being damaged means degradation in the quality of insulation, occurrence of partial discharges and ultimately breakdown of the insulation [1,2].

An important operational factor which threatens the cable insulation is the maximum operating temperature. General reasons for exceeding maximum operating temperature are poor feasibility studies, choosing closer design parameters to the maximum capacity of the cable and rapid growth in user demands. Another important factor is the presence of ‘hot spots’ at the bending points of the cable. Since the thermal interaction on these points accelerates the aging process, the operating period of the cable will be even shorter than estimated values if these hot spots are not detected or neglected. That is, transmission of the determined power in the specified duration and operation of the cable without any problem is related to the cable temperature. Therefore, the temperature profile must be monitored along the cable and real-time processing of temperature data must be achieved.

The conventional temperature detection method used in power cables is called the point temperature measurement

* Corresponding author. Tel.: +90 2244428179/1018; fax: +90 2244428021.

E-mail addresses: gunesy@uludag.edu.tr (G. Yilmaz), ekarlik@uludag.edu.tr (S.E. Karlik).

method. A thermocouple or a platinum resistance probe is required for every measurement point in this method [3]. Therefore, to obtain the temperature profile along the cable, a large number of sensors and fiber connectors are required. Moreover, integrated thermal behaviour of the cable can only be estimated by making some assumptions for different amounts of load and environmental conditions.

Furthermore, temperature values obtained by using mathematical models such as finite elements methods can only be consistent with real values with a maximum percentage of 80% or 90%. When optimistic assumptions are used in computations, there is a high risk of damage for the cable, which operates with predicted loads, because of the thermal reasons. On the other hand, pessimistic assumptions restrict the optimum use of the cable for economical means since they limit the present capacity. It is also very difficult for theoretical computations and simulations to predict environmental variations [4–7].

In this study, an optical fiber and distributed temperature sensing (DTS) method have been used to obtain the temperature profile along the cable. The term ‘distributed sensing’ defines a method in which only one detector receives data from a multiplicity of independent measurement points along the cable. In the distributed temperature sensing method, silica fiber behaves as a sensor itself. Therefore, there is no need for the devices of the conventional method since we benefit from characteristic properties of the fiber. The fibers used for the whole of the measurements are the silica fibers used in telecommunication applications and are therefore freely available. Using optical fiber as a sensing device has various advantages that come from the nature of fiber such as security in media that hold electrical and chemical risks, immunity to electromagnetic interference, high resistance to corrosions. Furthermore, it is also cost-effective for this application since there are large numbers of measurement points.

We describe DTS principles used in XLPE insulated power cable in Section 2. Section 3 is about the temperature sensing system configuration and experimental results. Finally in Section 4, we present simulation results for the temperature profile of a 10 km power cable under different operating conditions.

2. DTS principles used in XLPE insulated power cable

The most popular insulation used in production of power cable is cross-linked polyethylene abbreviated as XLPE. XLPE shows a more stable behaviour than normal polyethylene at high temperatures. Its ability in resisting to high temperatures ensures transmission of high currents. Continuous operation in 90 °C and a maximum temperature range of 250 °C for short duration indicate that XLPE is also resistant to high temperatures obtained under short-circuit conditions [8].

The most suitable expression of XLPE insulation ageing duration (τ) is described in the Zhurkov model [9]

$$\tau = \tau_0 \exp\left(\frac{U_0 - \chi E}{kT}\right) \quad (1)$$

where U_0 is the activation energy, τ_0 the inverse vibration frequency of material molecules, χ a structural parameter, E the applied electric field, k the Boltzmann constant and T is the temperature. It is clear from Eq. (1) that the value of temperature and its distribution in the cable is very important for a long reliable operating time.

The distributed sensing capabilities of optical fibers can be used to create various forms of intrinsic sensors where the modulation of optical carrier induced by the measurand occurs while the light remains guided within the fiber. The intrinsic fiber sensors are also distributed if the measurand acts over the whole length of fiber. Then, there are potentially thousands of independent measuring points along the fiber which give information about the measurand in a distributed manner.

The integration of the fiber into the power cable in the most suitable form has a great importance for the reliability of DTS. Ideally, the fiber must be located as close as possible to the cable conductor but this approach is not practical since the cable insulation must be split to reach the conductor. An important point about which one must make a decision is whether to include the fiber in the power cable construction or not. In this case, the fiber must overcome power cable production processes including various bending and high temperature operations. In this study, integration of optical fibers to power cables is implemented as being located in special non-magnetic tubes that are placed between screening wires of high voltage cables. The integration of optical fibers to 89/154 kV high voltage cables is shown in Fig. 1. Since such a fiber integration does not depend on production and implementation processes of the cable, there is no need



Fig. 1. Integration of optical fiber to 89/154 kV power cable.

for any variation in standard cable design and fibers located in tubes can be exchanged with new ones when it is required [10].

There are various sensing principles in DTS, e.g. Rayleigh, Raman and Brillouin scattering, mode coupling and optical Kerr effect. Among these, we are dealing with Raman scattering in combination with optical time domain reflectometry (OTDR) in this paper.

Although much research about reflectometry methods has been reported in the time domain, frequency domain and coherence domain for distributed sensors, the most popular technique is the optical time domain reflectometry (OTDR), which was first proposed by Barnowski and Jensen in 1976 as the first method for optical fiber distributed sensing [11]. Barnowski and Jensen determined the optical loss along the fiber by using back-scattered Rayleigh scattering.

In the OTDR method, light pulses are launched into the optical fiber. While light propagates in the fiber, a fraction of light scatters in a direction 180° to the propagation axis. This back-scattering is the combination of Rayleigh scattering caused by the density and structure of material and Raman and Brillouin scatterings occurred due to molecular and volumetric vibrations. The scattering sensitive to the measurand (distance, temperature, etc.) is filtered at the receiver by an interference filter and variation in the intensity of the filtered back-scattered light is determined as a fraction of the measurand.

The sensitivity of Rayleigh scattering is very low to temperature variations. Therefore, it is generally used to determine losses, bendings and inhomogeneities that occur in the cable. Raman and Brillouin scatterings are sensitive to temperature. Although it has a high temperature dependence, Brillouin scattering cannot be easily separated from Rayleigh scattering. This increases the cost of the receiver. However, Raman scattering has a sufficient temperature dependence to be used in distributed sensing and can be easily detected [12].

Effects of light scattering in optical fibers are classified according to the relation between frequencies of incident and scattered photons. When the frequencies of incident and scattered photons are equal, an elastic scattering occurs. Since a fraction of the optical power in one propagation mode is transferred linearly to another mode, Rayleigh scattering is an example of elastic scattering. Rayleigh scattering is a result of random inhomogeneities that occur in small scales with respect to the wavelength of light. These inhomogeneities exhibit fluctuations in the refractive index and are mainly because of density and composition variations placed in the silica during the cooling process. If frequencies of incident and scattered photons differ, this is a case of inelastic scattering, e.g. Raman scattering. In this case, frequencies of scattered photons shift from frequencies of incident photons to specific values. Frequency shifts are equal to the characteristic vibration frequencies of the molecules. Photons scattered to lower frequencies are called Stokes lines while photons scattered to higher frequencies are called anti-Stokes lines.

Stokes and anti-Stokes emissions of Raman scattering can be used to detect temperature profiles in conventional vitreous communication fibers. The ratio R_r of anti-Stokes to Stokes intensity in the back-scattered light is given by

$$R_r = \left(\frac{\lambda_S}{\lambda_A} \right)^4 \exp \left(\frac{hc\Delta\nu}{kT} \right) \quad (2)$$

where λ_S and λ_A are Stokes and anti-Stokes wavelengths, h the Planck's constant, c the speed of light in vacuum, $\Delta\nu$ the optical frequency shift, k the Boltzmann constant and T is the absolute temperature in Kelvin. This ratio has a magnitude of ~ 0.15 at room temperature and a temperature dependency of approximately $0.8\%/^\circ\text{C}$ in the range $0\text{--}100^\circ\text{C}$ [12].

Therefore, a measurement of the ratio of Stokes and anti-Stokes back-scattered light in a fiber should provide an absolute indication of the temperature of the medium, irrespective of the light intensity, the launch conditions, the fiber geometry and even the composition of the fiber. In practice, however, a small correction has to be made for the difference in fiber attenuation between the Stokes and anti-Stokes wavelengths.

While determining the temperature profile of the cable, the location of the point that sends the temperature datum must also be known. In the OTDR method, it is possible to determine the scattering point by measuring the duration of light reflection. If t is the propagation time of light in forward and backward direction, the distance traversed by the light can be computed by

$$d = \frac{ct}{2n} \quad (3)$$

where c is the speed of light in vacuum and n is the refractive index of the fiber.

3. Temperature sensing system configuration and experimental results

The block diagram of the DTS system that we used in our work is shown in Fig. 2. A neodymium doped pulse laser

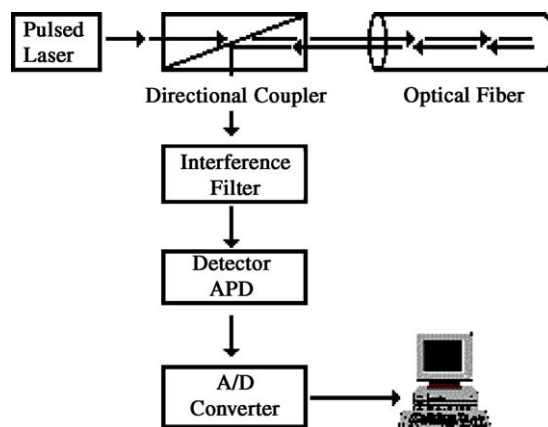


Fig. 2. Block diagram of DTS system.

generates pulses of duration 12.2 ns at a wavelength of 1320 nm. A directional coupler is used to separate the back-scattered signal from generated pulses. The scattered Raman signal is filtered by the interference filter and detected by a photodiode. The detected signal is then amplified and digitized by a high-speed analogue-to-digital converter. Digital averaging techniques improve the signal to noise ratio in a highly efficient manner prior to the data being sent to the display unit.

Parameters that affect the performance of the system shown in Fig. 2 can be described as follows:

- *Fiber length (spatial range)*: The maximum length of the fiber over which measurements can be made within the specified accuracy is defined as the spatial range. It is determined by the total two-way loss in the fiber and must include connectors as well as the fiber. Since the maximum fiber length can be determined by

$$L_{\max} = \frac{cT}{2n_{\text{gr}}} \quad (4)$$

where c is the speed of light in vacuum, T the pulse period and n_{gr} is the group refractive index of the fiber core. The spatial range is approximately equal to L_{\max} with an error of $\pm 1.14\%$ due to errors in T and n_{gr} .

- *Spatial resolution and sampling interval*: Spatial resolution is the distance between 10% and 90% of the temperature variation in the temperature versus distance graphic. DTS response to local temperature variations is determined with the help of this parameter. If the temperature variation occurs in a region smaller than the DTS spatial resolution, the measured temperature will be smaller than the real temperature by a ratio of temperature variation distance/spatial resolution. The spatial resolution can be computed with

$$\Delta z_{\min} = \frac{c\tau}{2n_{\text{gr}}} \quad (5)$$

where τ is the pulse duration.

Sampling interval is the distance between two measurement points and determines the total number of measurement points in the fiber sensor. In our measurements, the sampling interval is equal to the spatial resolution to be similar with the value used in simulations. Smaller sampling intervals give better location of temperature variations.

- *Temperature resolution*: It is the minimum discernable difference that the measurement system can interpret between two temperature values.
- *Measurement time*: It is the time required to obtain the temperature profile with a specific resolution of the fiber sensor. It includes detection and processing of the back-scattered signal.
- *Thermal response time*: The thermal response time of a sensor loop depends strongly on the cladding and cabling structure and on the quality of the thermal contact between the sensor loop and the conductor of the power cable whose

temperature is to be measured. In general, thermal response time is typically less than 0.5 s in the fiber.

Temperature resolution is an indication of the response of the measurement system to minimum temperature variations, while spatial resolution reflects the ability of the DTS to accurately locate and measure specific features of interest. Spatial resolution is critical for correctly assessing potential hot spots. A hot spot which occupies a fiber length which is less than the spatial resolution of the DTS instrument will not indicate its true amplitude.

Multi-mode step index fibers can be used for short spatial range and low spatial resolution while multi-mode graded index fibers and single-mode fibers can be chosen for long spatial range and high spatial resolution.

Whatever wavelength is selected, the most important design criteria of the source are the pulse width and the peak power of the laser. It is clear from Eq. (5) that pulse width is important in determining the spatial resolution. The importance of laser peak power is that the pumping power must be greater than a threshold value for occurrence of the stimulated Raman scattering. This threshold power can be computed by [13,14]

$$P_0^{\text{th}} = \frac{16A_{\text{eff}}}{L_{\text{eff}}g_{\text{R}}} \quad (6)$$

where g_{R} is the Raman gain constant (10^{-13} m/W) and A_{eff} and L_{eff} are the effective cross-sectional area and effective length of the fiber, respectively and can be computed by [13,14]

$$A_{\text{eff}} = \pi r^2 (0.65 + 1.619 f^{-3/2} + 2.879 f^{-6})^2 \quad (7)$$

$$L_{\text{eff}} = \frac{1}{\alpha_{\text{p}}} [1 - \exp(-\alpha_{\text{p}}L)] \quad (8)$$

where r is the fiber core radius, f the frequency, α_{p} the absorption constant of the pumping light and L is the fiber length. For example, Raman threshold power will be 1.22 W for a fiber sensor that has an effective cross-sectional area of $60 \mu\text{m}^2$ and an effective length of 7.87 km.

Our sensing system has a temperature resolution of 1°C and spatial resolution of 1.22 m. The source output power, which is 3 W, is greater than the threshold power value of 2.45 W. Using the system shown in Fig. 2, measurements were performed on two 154 kV power cables of lengths 126 and 412 m under different medium conditions.

The temperature profile obtained from measurements performed with optical fiber DTS method on a 126 m long 154 kV power cable is shown in Fig. 3. In the first 16 h of the total test duration, current flowed through the cable and temperature variations of the cable were detected for 48 h. In Fig. 3, graphic sections I, III, V and VI show temperature profiles of buried cable sectors while sections II and IV exhibit temperature profiles of cable sectors placed in ducts. In every case, cable temperature did not exceed 90°C , which is the typical maximum operating temperature of XLPE cables, and

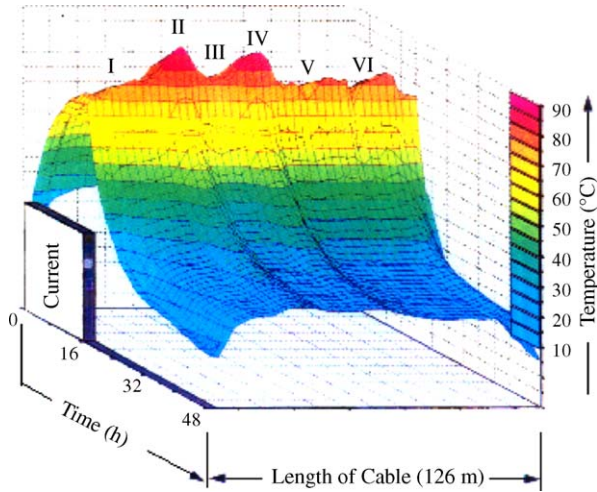


Fig. 3. Temperature profile obtained from 154 kV XLPE power cable with a length of 126 m.

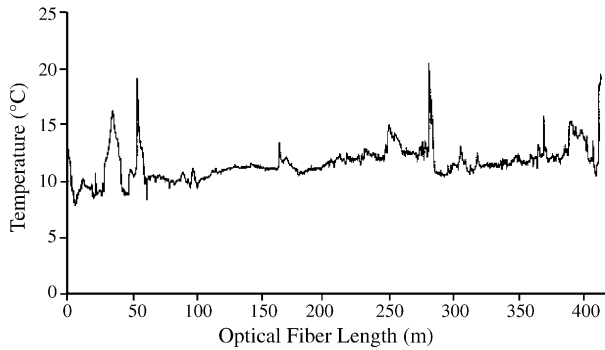


Fig. 4. Temperature profile measured on 154 kV XLPE power cable with a length of 412 m.

only cable sectors which were placed in ducts reached to this value. The maximum temperature reached by buried sectors was about 80 °C.

The temperature profile obtained from measurements performed on 154 kV XLPE power cable with a length of 412 m is shown in Fig. 4. During the experiment, different ambient temperatures were formed at different regions along the cable. The temperature profile in Fig. 4 shows these ambient temperatures with a temperature resolution of ± 1 °C.

4. Simulations

In the case of high spatial resolution sensors where multi-mode parabolic gradient index fibers or single-mode fibers are used, Raman Stokes power, which originates at any location z along the fiber, measured at the fiber input ($z=0$) at a time t after a pulse is transmitted from the laser source can be described by [15]

$$P_S(t) = \hat{P}_0 \left(\frac{c\tau}{n_{gr}} \right) \wp_S \Gamma_S \frac{1}{2\alpha_{P,S}} \left[1 - \exp \left(-\alpha_{P,S} \frac{ct}{n_{gr}} \right) \right] \quad (9)$$

where \hat{P}_0 is the source power, c the speed of light in vacuum, τ the pulse duration, n_{gr} the group refractive index in the fiber core, \wp_S the Bose–Einstein factor for the Stokes band, Γ_S the Raman Stokes capture coefficient, $\alpha_{P,S}$ the effective power attenuation coefficient for the Stokes wave and t is the time.

Similarly, Raman anti-Stokes power, which originates at any location z along the fiber, measured at the fiber input ($z=0$) at a time t after a pulse is transmitted from the laser source can be described by [15]

$$P_{AS}(t) = \hat{P}_0 \left(\frac{c\tau}{n_{gr}} \right) \wp_{AS} \Gamma_{AS} \frac{1}{2\alpha_{P,AS}} \times \left[1 - \exp \left(-\alpha_{P,AS} \frac{ct}{n_{gr}} \right) \right] \quad (10)$$

where \wp_{AS} is the Bose–Einstein factor for the anti-Stokes band, Γ_{AS} the Raman anti-Stokes capture coefficient, $\alpha_{P,AS}$ the effective power attenuation coefficient for the anti-Stokes wave. \wp_S and \wp_{AS} of Eqs. (9) and (10) can be computed using

$$\wp_S = \frac{1}{1 - \exp(-\Delta E/kT)} \quad (11)$$

and

$$\wp_{AS} = \frac{\exp(-\Delta E/kT)}{1 - \exp(-\Delta E/kT)} \quad (12)$$

respectively, where k is the Boltzmann constant, T the absolute temperature of fiber and ΔE is the difference between molecular energy states E_2 and E_1 of Raman scattering.

$\alpha_{P,S}$ and $\alpha_{P,AS}$ of Eqs. (9) and (10) can be computed with

$$\alpha_{P,S} = \frac{\alpha_P(\lambda_0) + \alpha_P(\lambda_S)}{2} \quad (13)$$

and

$$\alpha_{P,AS} = \frac{\alpha_P(\lambda_0) + \alpha_P(\lambda_{AS})}{2} \quad (14)$$

respectively, where $\alpha_P(\lambda_0)$ is the attenuation coefficient of the pulse laser in the fiber at the wavelength λ_0 , $\alpha_P(\lambda_S)$ the power attenuation coefficient at the Stokes wavelength and $\alpha_P(\lambda_{AS})$ is the coefficient at the anti-Stokes wavelength. Attenuation coefficients for parabolic gradient index multi-mode fiber and single-mode fiber at different wavelengths are given in Table 1.

Capture coefficients Γ_S and Γ_{AS} for parabolic gradient index multi-mode fiber and single-mode fiber at different Stokes and anti-Stokes wavelengths are given in Table 2.

Taking the ratio of Eqs. (10) and (9) and making some simplifications, Eq. (2) can be obtained. By using the pulse response measured with OTDR, temperature can also be computed using

$$T(z_q) = \frac{\Delta E}{k \ln[(h_S(t)/h_{AS}(t))(\lambda_S/\lambda_{AS})^4 \exp(\Delta\alpha_P z_q)]} \quad (15)$$

where $h_S(t)$ and $h_{AS}(t)$ are detected Stokes and anti-Stokes pulse responses and $\Delta\alpha_P$ is 1.3×10^{-6} for single-mode fiber.

Table 1

Attenuation coefficients for parabolic gradient index multi-mode fiber and single-mode fiber at different wavelengths

λ (nm)	Parabolic gradient index multi-mode fiber, α (dB/km)	Single-mode fiber, α (dB/km)
810	3.00	2.40
840	2.40	1.90
872	2.00	1.60
1248	0.60	0.40
1320	0.40	0.33
1401	0.90	0.40
1451	0.50	0.25
1550	0.35	0.20
1663	0.37	0.22

For detailed information about the above equations and tables of this section, please refer to [15].

Simulations about distributed temperature sensing with a fiber sensor mounted in a 154 kV power cable, whose length is 10 km, were made with MATLAB. In these simulations, back-scattered Stokes and anti-Stokes signals were obtained as well as the temperature profile. A single-mode fiber operating at a wavelength 1320 nm was used. Required parameters of such a fiber are given in Tables 1 and 2. Parameters used in simulations are as follows:

- Transmitted pulse duration: $\tau = 12.2$ ns.
- Maximum power of pulse laser: $\hat{P}_0 = 3$ W.
- Fiber length: $L = 10\,000$ m.
- Spatial resolution (computed with Eq. (5)): $\Delta z_{\min} = 1.22$ m.
- Number of discrete points detected with 1.22 m spatial resolution:

$$\frac{\text{fiber length}}{\text{spatial resolution}} = \frac{10\,000}{1.22} = 8196$$

With the help of Eqs. (11) and (12), φ_S and φ_{AS} coefficients can be computed depending on the temperature of the scattering point of the light.

Raman Stokes and anti-Stokes capture coefficients for single-mode fiber were found as $\Gamma_{S,\text{single}}(1320\text{ nm}) = 4.28 \times 10^{-10}$ and $\Gamma_{AS,\text{single}}(1320\text{ nm}) = 5.39 \times 10^{-10}$ by using Table 2.

With the help of Table 1, effective power attenuation constants for Stokes and anti-Stokes wavelengths were computed as $\alpha_{P,S} = \alpha_{P,AS} = 0.365$ dB/km.

Table 2

Capture coefficients at different Stokes and anti-Stokes wavelengths

λ_0 (nm)	840	1320	1550
λ_S (nm)	872	1401	1663
λ_{AS} (nm)	810	1248	1451
$\Gamma_{S,\text{grad}} (\times 10^{-10} \text{ m}^{-1})$	87.7	13.2	6.63
$\Gamma_{AS,\text{grad}} (\times 10^{-10} \text{ m}^{-1})$	118	20.9	11.4
$\Gamma_{S,\text{single}} (\times 10^{-10} \text{ m}^{-1})$	–	4.28	3.04
$\Gamma_{AS,\text{single}} (\times 10^{-10} \text{ m}^{-1})$	–	5.39	4.00

Back-scattered Stokes and anti-Stokes signals were found using Eqs. (9) and (10). Gaussian noise was added to the detected Stokes and anti-Stokes signals. To obtain the distributed temperature on the power cable, Eq. (15) was used.

In the simulation program written for distributed temperature measurement of the long range power cable with fiber sensor, different medium conditions were formed along the cable as follows:

- Cable connection points repeated every 1000 m with the first one being at the 1000th meter.
- Bedding in a 20 m duct at the 2500th meter.
- Cross-connections with other cables at 3800th and 6700th meters.
- Bedding in 100 m ducts at 5500th and 7500th meters and cross-connections with other cables inside these ducts at 5550th and 7550th meters.

The simulated temperature profile of 154 kV power cable is shown in Fig. 5. It is clear in Fig. 5 that cable connection points, cross-connection points with other cables and bedding in ducts cause hot spots to occur on the cable. The average temperature is approximately 80°C excluding hot spots. Cable connection points raise the temperature locally to 90°C but the most critical temperature increments that must be monitored are due to cross-connections with other cables and bedding in ducts. This may be analyzed by zooming to the circled parts of Fig. 5, the first one of which is shown in Fig. 6.

As shown in Fig. 6, bedding the power cable in a 20 m duct causes the temperature to exceed 85°C . This temperature variation is in good agreement with our measured results in short cables. However, the temperature is still below the value due to cable connection points.

The second circled part of the graphic in Fig. 5 may be examined more closely as shown in Fig. 7, which illustrates the simulated temperature profile of the cable sector that passes through a 100 m duct starting at the 5500th meter and cross-connects with another power cable in the duct at the 5550th meter.

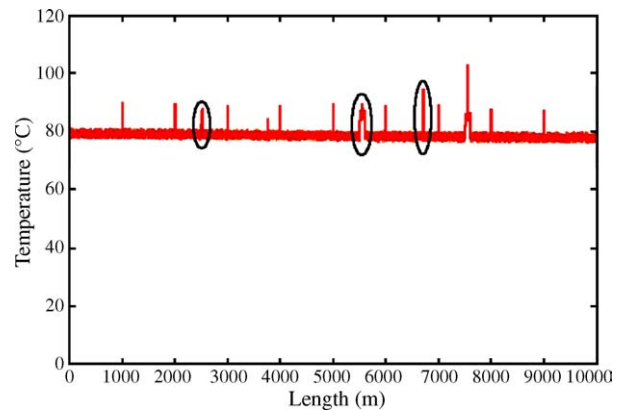


Fig. 5. Simulated temperature profile of 154 kV power cable.

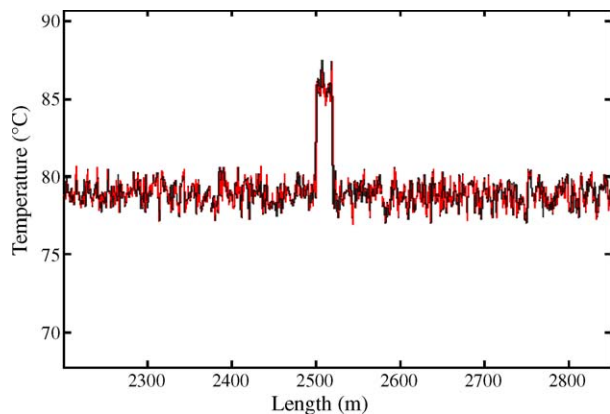


Fig. 6. Temperature variation at the 2500th meter due to bedding in a 20 m duct.

Comparing to Fig. 6, it is clear that the temperature exceeds 85°C in the duct and locally rises to 88°C , which is very near in value to the critical temperature 90°C , at the cross-connection point. The temperature increment depends on the thermal interaction with the power cable at the cross-connection point as well as the length, diameter and thermal conductivity of the duct. Under similar conditions, cable temperature reaches to 105°C – a higher value than the critical temperature 90°C – at 7550th meter as shown in Fig. 5. Zooming in the third circled part of the graphic in Fig. 5, Fig. 8 can be obtained.

Fig. 8 shows the increment in the temperature of 154 kV power cable due to a cross-connection with another power cable at the 6700th meter. The temperature exceeds the critical value and is approximately 93°C . This is because of the thermal interaction between cables at the cross-connection point. Comparing to Fig. 7, it is obvious that the temperature, and consequently the load, of the cable that cross-connects with our 154 kV cable at the 6700th meter is more than that of the one at the 5550th meter. This is indeed the case that we considered for our simulation model. Besides the instantaneous current that flows through cross-connected cables, the

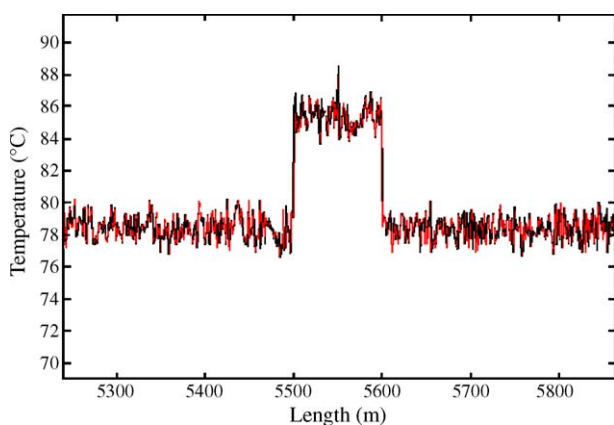


Fig. 7. Temperature variation due to bedding in a 100 m duct at the 5500th meter and cross-connection with another cable at the 5550th meter.

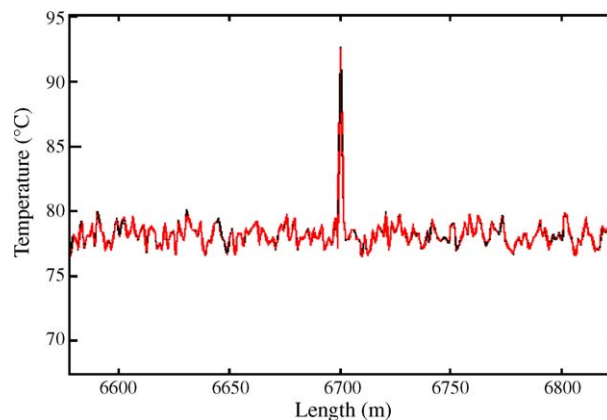


Fig. 8. Temperature variation at the 6700th meter due to a cross-connection with another power cable.

temperature increment depends also on the degree of cross-connection angle and the distance between the conducting centers of cables.

5. Conclusion

In this study, a distributed temperature sensing system based on the temperature-sensitive Raman scattering has been proposed for a 154 kV XLPE insulated power cable. Integration of the optical fiber to the power cable has been achieved. Parameters that affect the receiver performance have been analyzed. Using DTS method, temperature measurements have been performed on two power cables with lengths of 126 and 412 m under different conditions such as during and after a current flow through buried cables and cables placed in ducts. Also, simulations have been made for long range (10 km) 154 kV XLPE insulated power cables. In these simulations, effects of cross-connections, cable connection points and ducts on temperature variations have been analyzed. Experimental and simulation results have shown a good agreement between real and model temperature values, e.g. there is a 5°C variation between maximum temperature values of buried cable sectors (I and III) and cable sectors placed in ducts (II and IV) in measurements while 80°C average temperature of the cable rises to 85°C due to bedding in a 20 m duct in simulations. These show that DTS is a reliable method to obtain temperature profiles of both short and long range power cable systems.

References

- [1] Y. Asada, Y. Maruyama, A study of insulation shrinkback in cross-linked polyethylene cables, JICABLE Paper B4.3 (1987) 264–269.
- [2] R.J. Densley, R.J.R. Bartnikas, B. Bernstein, Multiple stress of aging of solid-dielectric extruded dry-cured insulation systems for power transmission cables, IEEE Trans. Power Delivery 9 (1) (1994) 559–571.

- [3] S. Nakamura, S. Morooka, K. Kawasaki, Conductor temperature monitoring system in underground power transmission XLPE cable joints, *IEEE Trans. Power Delivery* 7 (4) (1992) 1688–1697.
- [4] D.A. Douglass, A.A. Edris, Real-time monitoring and dynamic thermal rating of power transmission circuits, *IEEE Trans. Power Delivery* 11 (3) (1996) 1407–1418.
- [5] P. Caramia, A. Losi, M. Russo, Conductor temperature estimation of underground cables, *JICABLE Paper B8.3* (1999) 571–576.
- [6] D.A. Douglass, D.C. Lawry, A.A. Edris, E.C. Bascom, Dynamic thermal ratings realize circuit load limits, *IEEE Comput. Appl. Power* 13 (1) (2000) 38–44.
- [7] C. Garrido, A.F. Otero, J. Cidras, Theoretical model to calculate steady-state and transient ampacity and temperature in buried cables, *IEEE Trans. Power Delivery* 18 (3) (2003) 667–678.
- [8] N.H. Malik, A.A. Al-Arainy, M.I. Quereshi, *Electrical Insulation in Power Systems*, Marcel Dekker Inc., New York, 1998, pp. 462–463.
- [9] F. Aras, H.S. Varol, Correlation of ampacity and insulation life time of XLPE power cable under thermal/electrical stresses, in: *Proceedings of the Sixth International Conference on Dielectric and Related Phenomena*, Spala, Poland, 2000, p. 97.
- [10] G. Yilmaz, S.E. Karlik, A real-time temperature monitoring application on high voltage cables with optical fiber sensors, in: *Proceedings of the Ninth National Congress of Electrical–Electronics and Computer Engineering*, Izmit, Turkey, 2001, pp. 30–34 (in Turkish).
- [11] M.K. Barnowski, S.M. Jensen, Fiber waveguides: a novel technique for investigating attenuation characteristics, *Appl. Opt.* 15 (9) (1976) 2112–2115.
- [12] *Distributed Temperature Sensing Systems (Fibre Optic) Catalogue*, York Sensors Ltd., 1999.
- [13] A. Kersey, Distributed and multiplexed fiber optic sensors, in: E. Udd (Ed.), *Fiber Optic Sensors: An Introduction for Engineers and Scientists*, Wiley Series, Wiley, New York, 1991, pp. 327–340.
- [14] E. Musayev, *Optoelectronic Circuits and Systems*, Birsen Press, Istanbul, 1999, pp. 68–69 (in Turkish).
- [15] M.A. Farahani, T. Gogolla, Spontaneous Raman scattering in optical fibers with modulated probe light for distributed temperature Raman remote sensing, *J. Lightwave Technol.* 17 (8) (1999) 1379–1391.

Biographies

Gunes Yilmaz received his BSc and MSc degrees in electronics and communication engineering from Varna Technical University, Varna, Bulgaria in 1980 and 1985, respectively. He received his PhD degrees in electrical engineering from Sofia Technical University, Sofia, Bulgaria in 1989 and in electronics and communication engineering from Istanbul Technical University, Istanbul, Turkey in 1994. He worked as an R&D manager for Turk Siemens Cables and Systems A.S. between 1990 and 1998. Between 1998 and 2002 he was with Turk Pirelli Cables and Systems A.S. as an R&D and quality systems manager. Currently, he is an associate professor in Electronics Engineering Department of Uludag University, Bursa, Turkey. Up to now, he supervised 40 different R&D projects and worked in the organization of six national and three international conferences as a co-chairman or a technical committee member. He is the author or co-author of more than 60 scientific papers and holds two international patents. His research interests include digital communications, optical fiber communication systems, measurement techniques and fiber sensors.

Sait Eser Karlik received his BSc degree in electronics and telecommunication engineering from Istanbul Technical University, Istanbul, Turkey in 1997 and his MSc degree in electronics engineering from Uludag University, Bursa, Turkey in 1999. Currently, he is a research assistant and working toward his PhD degree at Electronics Engineering Department of Uludag University. His research interests involve optical fiber communication systems, fiber sensors and high-speed local area networks.